AD-A063 869 ELECTROCHEMICAL TECHNOLOGY CORP SEATTLE WASH F/G 11/6
FORMATION OF SALT FILMS DURING PASSIVATION OF IRON.(U)
DEC 78 T R BECK N00014-76-C-0495
UNCLASSIFIED NL

1 OF 1
AD
A063 869

END
DATE
FILMED
3--79
DDC

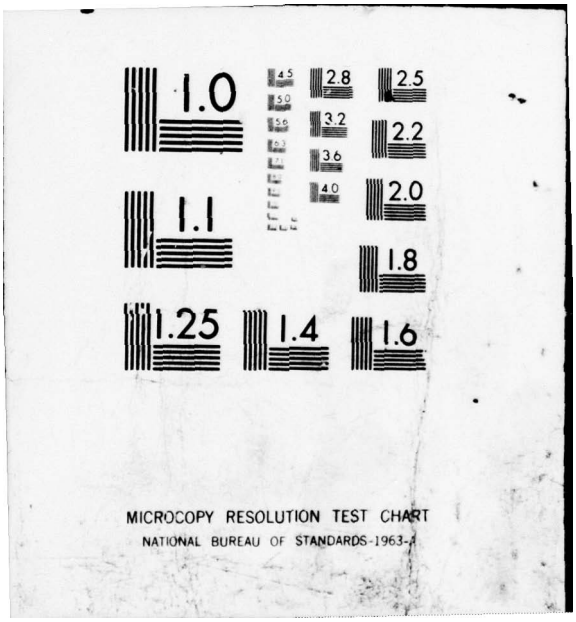
1.0
1.1
1.25
1.4
1.6
1.8
2.0
2.2
2.5
2.8
3.2
3.6
4.0
4.5
5.0
5.6
MICROCOPY RESOLUTION TEST CHART
NATIONAL BUREAU OF STANDARDS-1963-A

LEVEL II

12

Contract N00014-76-C-0495
(15)

(6)

FORMATION OF SALT FILMS DURING PASSIVATION OF IRON.

Manuscript

(10)
THEODORE R. BECK
ELECTROCHEMICAL TECHNOLOGY CORP.
3935 LEARY WAY N.W.
SEATTLE, WA 98107
(206) 632-5965

(9)

INTERIM REPORT FOR PERIOD MARCH 1977 — FEB 1978,

Prepared for

OFFICE OF NAVAL RESEARCH
800 North Quincy Street
Arlington, VA 22217

(11) Dec 1978 (12) 34 p.

Unclassified

SECURITY CLASSIFICATION OF THIS PAGE (When Data Entered)

REPORT DOCUMENTATION PAGE		READ INSTRUCTIONS BEFORE COMPLETING FORM
1. REPORT NUMBER	2. GOVT ACCESSION NO.	3. RECIPIENT'S CATALOG NUMBER
4. TITLE (and Subtitle) Formation of Salt Films during Passivation of Iron		5. TYPE OF REPORT & PERIOD COVERED Technical Report March, 1977 - March, 1978
		6. PERFORMING ORG. REPORT NUMBER
7. AUTHOR(s)		8. CONTRACT OR GRANT NUMBER(s) N00014-76-C-0495
9. PERFORMING ORGANIZATION NAME AND ADDRESS Electrochemical Technology Corp. 3935 Leary Way N.W. Seattle, WA 98107		10. PROGRAM ELEMENT, PROJECT, TASK AREA & WORK UNIT NUMBERS
11. CONTROLLING OFFICE NAME AND ADDRESS Office of Naval Research Materials Science Division Arlington, VA 2217		12. REPORT DATE December, 1978 13. NUMBER OF PAGES 31 34
14. MONITORING AGENCY NAME & ADDRESS(if different from Controlling Office)		15. SECURITY CLASS. (of this report) Unclassified 15a. DECLASSIFICATION/DOWNGRADING SCHEDULE

16. DISTRIBUTION STATEMENT (of this Report)

17. DISTRIBUTION STATEMENT (of the abstract entered in Block 20, if different from Report)

Reproduction in whole or part is permitted for any purpose of the United States Government. Distribution is unlimited.

18. SUPPLEMENTARY NOTES

Manuscript to be submitted to the Journal of The Electrochemical Society. This paper was presented at Electrochemical Society, Abstract No. 128, Pittsburgh, Pa., Oct. 15-20, 1978.

19. KEY WORDS (Continue on reverse side if necessary and identify by block number)

Corrosion, kinetics, mass transport, oscillation, iron, passivation.

20. ABSTRACT (Continue on reverse side if necessary and identify by block number)

Pure iron in the form of a shielded electrode facing upward was anodically polarized in hydrochloric, perchloric, and sulfuric acid solutions. Ferrous salt films formed in all three electrolytes at potentials and current densities above threshold values determined by mass transport. In perchloric and sulfuric acids, oxide passivation occurred underneath the salt film at potentials above the passivation potential. Analysis of kinetic and transport conditions under and within these salt films indicated

DD FORM 1 JAN 73 1473 EDITION OF 1 NOV 65 IS OBSOLETE

Unclassified

SECURITY CLASSIFICATION OF THIS PAGE (When Data Entered)

that salt films are necessary precursors to oxide passivation in perchloric and sulfuric acid solutions. Oscillatory phenomena during passivation of iron can be explained by formation and dissolution of salt films coupled to pH changes under the salt film due to electrolytic migration.

FORMATION OF SALT FILMS DURING PASSIVATION OF IRON

Theodore R. Beck*

Electrochemical Technology Corp.
3935 Leary Way N.W., Seattle, Washington 98107

ABSTRACT

Pure iron in the form of a shielded electrode facing upward was anodically polarized in hydrochloric, perchloric, and sulfuric acid solutions. Ferrous salt films formed in all three electrolytes at potentials and current densities above threshold values determined by mass transport. In perchloric and sulfuric acids, oxide passivation occurred underneath the salt film at potentials above the passivation potential. Analysis of kinetic and transport conditions under and within these salt films indicated that salt films are necessary precursors to oxide passivation in perchloric and sulfuric acid solutions. Oscillatory phenomena during passivation of iron can be explained by formation and dissolution of salt films coupled to pH changes under the salt film due to electrolytic migration.

Key words: Corrosion, kinetics, mass transport, oscillation.

*Electrochemical Society Active Member

This manuscript
to be submitted to the
Journal of The Electrochemical Society

Numerous descriptions are given in the literature of formation of salt films on metals during the passivation process in acid and salt solutions. W. J. Müller (1, 2) states that if the oxide film on iron is destroyed or disturbed in sulfuric acid electrolytes, there results a film of ordinary ferrous sulfate heptahydrate, which changes at potentials in excess of about 2 volts (cell voltage) to a film of higher oxide of iron. He used anodes facing up, shielded with a piece of rubber tubing to avoid convection effects, so that mass transport was only by diffusion and migration.

Bartlett (3) made extensive observations of current oscillations during passivation of iron in 2N H_2SO_4. He attributed the oscillations to transport of HSO_4^- and perhaps due to a reaction between Fe^{++} and HSO_4^- forming a precipitate which impedes the flow of current. Bartlett and Stephenson (4) subsequently measured polarization curves for this system against a calomel reference electrode and showed that the periodic phenomena occurred in a region of potential at the onset of passivity. They also observed under a microscope that films formed on the iron anodes in the active region prior to passivity.

Serra and Feliu (5) anodically polarized iron in sulfuric acid, sodium sulfate, and ferrous sulfate at various constant currents and observed the time to (salt) passivation as a function of current density. They found that above a certain critical current density the product of current density and square root of time to passivation was constant, in agreement with Sand's equation (6) for unsteady-state diffusion. They calculated a supersaturation factor of about two for $FeSO_4$ to precipitate from H_2SO_4 solutions. Froment, et al., (7) also observed ferrous sulfate crystals on the surface of active

iron in sulfuric acid. Schwabe (8) indicated that a primary salt layer may be a necessary precursor to the passivation of iron in sulfuric acid.

Williamson and Hines (9) and Hines (10) studied passivation by sulfation of mild steel in strong sulfuric acid; these processes were of practical interest for anodic protection. With application of a step anodic potential, Hines observed a complex current-density transient consisting of an initial peak and rapid decay followed by a rise and a second lower peak and subsequent slower decay. Tousek and Prazak (11) also studied passivation of iron in concentrated sulfuric acid. They believed the ferrous sulfate films to be hydrated in lower concentration H_2SO_4 but to be anhydrous at above 86% H_2SO_4.

Pigeaud and Kirkpatrick (12) made microscopic observations of iron anodically polarized in 1N H_2SO_4. They discuss a ring of greatly increased reflectance to grow in toward the center from the circumference of the specimen; they attributed this ring to colloidally dispersed ferrous hydroxide. Abakumova and Milyutin (13) discuss the formation of a ferrous sulfate film which retards anodic dissolution of iron in sulfuric acid (pH=0) prior to oxide formation.

Lorenz (14) made interesting studies of supersaturation of metal salt solutions prior to salt precipitation. Beck (15) also discussed formation of salt films on metals under anodic dissolution and calculated supersaturation ration of 1 to 5 times saturation for precipitation for various metals. Kuo and Landolt (16) describe a rotating disc study of anodic dissolution of iron in concentrated chloride media. The dissolution current density was mass transport limited by Fe^{++} away from the anode and the Fe^{++} concentration

at the surface corresponded to saturation. These authors (17) also showed that supersaturation occurs with a constant-current step applied to a shielded iron electrode in concentrated chloride solutions before $FeCl_2$ precipitates. Hoar (18) and Vermilyea (19) present general reviews on anodic behavior of metals. Kolotyrkin (20) and Rosenfeld (21) mention formation of salt films during passivation of metals.

The present study was initiated to obtain data to test a model (22) for precipitation and dissolution of salt films occurring during the passivation of active metals.

Experimental

The experiments described in this paper were all carried out with shielded (pit) electrodes, similar to those of Müller (1, 2), in order to obtain uniform current densities. The geometry is shown in Fig. 1. Rectangular 0.16 x 0.32 cm cross section rods of zone-refined iron* were cast into epoxy resin. They were operated in the anode-facing-up position in order to obtain hydrodynamic stability. Visible events on the surface of the anode could be observed through a 60X binocular microscope above the cell. Prior to each experiment, the anode was corroded on the end to a depth of greater than 0.1 cm in order to obtain a relatively uniform current density. Under the condition of a salt layer in the pit, the metal surface could be electropolished very smooth and flat.

A two-dimensional representation of primary current-density distribution across the width for the shielded electrode for several depths is given in

---

* Provided by courtesy of the American Iron and Steel Institute.

Fig. 2. The curves were developed by measuring equipotential lines on conducting paper cut out to the shape of the electrolyte cross section. The electrodes of silver conductive paint were applied at the appropriate edges of the conducting paper, and a dc potential was applied between them. Because of symmetry, only a half width of electrodes and electrolyte was required, so that the pit centerline was one edge of the conducting paper. An electrometer was used to measure potentials. Relative current density was calculated from the reciprocal of the distance from the anode to the closest measured equipotential curve. Results in Fig. 2 show that current density for a pit with depth equal to ¼ the width is relatively uniform in contrast to infinite primary current density at the edge of an electrode flush to the surface of the insulating resin.

In the analysis of the experimental data, it is important to know the relation of anode current density to ohmic drop in solution. The solution ohmic drop may be divided into two parts, that in the pit,

$$\Delta\phi_i = \frac{id}{\kappa} \tag{1}$$

and that outside of the pit, which may be approximated by hemispherical conduction to a counter electrode at infinity (23),

$$\Delta\phi_o = \frac{ir}{\kappa} \tag{2}$$

Combining 1 and 2, the total solution potential drop is in the electrolyte approximately

$$\Delta\phi_e \approx \frac{i}{\kappa}(d + r) \tag{3}$$

the approximation being due to matching current densities at the mouth of the pit. For a rectangular section, r will be replaced by a $\sqrt{\ell w}$,

$$\Delta\phi_e \approx \frac{i}{\kappa}\,(d + a\sqrt{\ell w}) \qquad (4)$$

In practice, if the counter electrode and reference electrode are more than 10 electrode widths from the pit, they may be considered at infinity within 5% error.

In the experiments, the platinum counter electrode and saturated calomel reference electrodes were 2 to 3 cm from the pit opening to be out of the way for observing the pit with the microscope. The depth of electrolyte over the pit mouth was about 1 cm. A model 68TS3 Wenking potentiostat was used for potentiostatic and galvanostatic experiments. In the potentiostatic experiments, the potential was stepped from the mixed potential to the anodic potential of interest. Before each anodic step, the pit was flushed out with an eyedropper to obtain a uniform concentration of bulk solution in the pit. The solutions were made from ACS-specification perchloric and sulfuric acids and distilled water. Potentials were converted to the standard hydrogen scale in this paper by adding 0.24 V.

Results and Discussion

Hydrochloric Acid Electrolyte.--Potentiodynamic current density-time curves for iron in 6N HCl are given in Fig. 3. A partial passivation occurs by precipitation of $FeCl_2$ (17), but oxide passivation does not occur in this electrolyte. Current densities at times greater than 1 sec. were obtained from an XY plotter and at times less than 1 sec. from a storage oscilloscope.

At the knees of the curves, e.g., at the point denoted by τ^*, crystals could be seen starting to grow from the periphery of the metal anode toward the center. The current density decayed as the crystals spread toward the

center of the anode. Nucleation at the edges may be ascribed to the slightly higher current density there and thus higher salt concentration in solution. The current density reached a minimum when the surface was completely covered with crystals. The current density then increased, passed through a maximum, and subsequently decayed as the $-\frac{1}{2}$ power of time. In the region of current rise, the needle-like crystals appeared to dissolve. The unsteady-state crystals precipitated from solution were apparently replaced by a steady-state salt film, different in structure and/or thickness.

Initial current density is linear with potential and is limited primarily by ohmic drop in solution (equation 4). The slight decrease in current density prior to τ^* can be attributed to concentrated, lower-conductivity, salt solution next to the anode surface. If step constant currents are applied to the electrode, the potential goes to a level determined by the ohmic resistance (equation 4) and then suddenly increases at salt passivation at a time, τ_p. The line of slope approximately $-\frac{1}{2}$ just above the knees of the potentiostatic curves in Fig. 3 was determined from constant current experiments.

The time to reach saturation concentration of $FeCl_2$ at the surface can be calculated from Sand's equation (6,17),

$$i = \tfrac{1}{2}zFC_s\sqrt{\frac{\pi D}{\tau_s}} \qquad (5)$$

in which $z = 2$, $C_s = 1.82 \times 10^{-3}$ mole/cm^3 in 6N HCl (17) and $D = 0.85 \times 10^{-5}$ cm^2/sec (17). This is the dashed line with slope = $-\frac{1}{2}$ plotted from 0.1 to 2 sec. in Fig. 3. The experimental line for i versus τ_p is above Sand's equation for saturation concentration by a factor of 2.6, indicating a supersaturation ratio of 2.6 for nucleation of salt precipitation. Kuo

and Landolt (17) observed a ratio of 2.

The final current density decay at a slope of $-\frac{1}{2}$ can be attributed to unsteady-state mass transport of Fe^{++} from the metal surface at which $FeCl_2$ is saturated. Considering diffusion only, this limiting current density can be described by (24),

$$i_L = zFC_s\sqrt{\frac{D}{\pi\tau}} \tag{6}$$

The above parameter values (for equation 5) in equation 6 give the dashed line plotted from 1 to 10^3 sec. in Fig. 3. The experimental data are about 40% above the line for equation 6, indicating that electrolytic migration of Fe^{++} is not negligible in this case, even in 6N HCl. Equation 6 may be expected to hold until the Fe^{++} penetrates the solution to the mouth of the cavity. This time required is approximately

$$\tau = \frac{d^2}{D} \tag{7}$$

which for a depth of 0.1 cm is about 10^3 sec. Thereafter, further current density decay is by deepening of the cavity by metal dissolution.

Perchloric Acid Electrolyte.--Potentiodynamic scans in the anodic and cathodic direction for iron in 5N $HClO_4$ are shown in Fig. 4. The anodic scans were started in the hydrogen evolution region and passed through the mixed potential to the anodic region. The anodic current density followed Tafel behavior up to about 0.1 A/cm^2. This region is not of interest in the present work and has been extensively studied by others (25-29); it will not be considered further here. Above 0.1 A/cm^2, the current density was limited primarily by ohmic resistence in solution (equation 4).

At about 0.7 A/cm^2, for the potential sweep speed of 1.6 V/min shown in

Fig. 4, the current density began to deviate from the linear ohmic relationship, and it subsequently peaked at about 0.9 A/cm^2. Just before the peak, light-green needle-like crystals could be seen growing from the periphery toward the center of the metal anode. Complete coverage by crystals occurred at the subsequent minimum in current density at about 0.3 A/cm^2.

The current density then increased to about 0.45 A/cm^2 and subsequently decreased slowly until oxide passivation occurred at about 0.6 V. The needle-like crystals were seen to start to disappear at the minimum and were gone when the current reached the plateau. The layer of crystals precipitated from solution next to the anode was apparently replaced by a steady-state layer of different crystal structure and/or thickness as in HCl solution. These types of maxima and minima have been reported previously for iron (10) and for copper (30). In the plateau region, the current density is limited by mass transport of ferrous ion as in HCl solution.

If the pit is flushed out with an eyedropper at potentials below the passivation potential, the current density rises to the ohmic limit (equation 4) and subsequently decays through the minimum and plateau regions. Above the oxide passivation potential, the iron does not become active by flushing the pit with bulk solution.

On a negative potential sweep, starting from the passive potential region, the iron surface suddenly depassivates at the passivation potential. The current density rises to the ohmic limit, decays to the minimum, rises and goes through a second lower maximum, and decays again at a lower rate. When the potential intersects that of the ohmic limited current density, the current density then decreases according to equation 4. The current

density is slightly below ohmic limited values for the positive sweep because the pit is now slightly deeper and has a layer of lower-conductivity, high-concentration $Fe(ClO_4)_2$ solution next to the metal surface. The concentrated, lower-acidity, $Fe(ClO_4)_2$ solution also suppresses hydrogen evolution. Flushing the pit causes hydrogen evolution to increase at potentials more negative than -0.1 V.

Application of step potentials or step current densities gives additional information more amenable to quantitative interpretation. Current density transients for step potentials from the mixed potential in 5N $HClO_4$ are shown in Fig. 5. At potentials of zero volts and above, the current densities were constant at the ohmic limit until the needle salt crystals appeared; then the current densities decayed. Passivation times for constant currents are shown as the line with about $-\frac{1}{2}$ slope above the knees of the constant potential experiments. The dashed Sand's-equation line is also plotted for saturation concentration (31) of $Fe(ClO_4)_2$ in 5N $HClO_4$; saturation was calculated to be 2.0×10^{-3} mole/cm^3. The supersaturation ratio is 2.2 to 3 for the experimental data.

As shown in Fig. 5, at potentials below the passivation potential, the current density decays through the minimum and rises to a lower maximum and decays as in the potentiodynamic experiments. The needle crystals disappeared at the minimum.

At potentials above the passivation potential, the current continues to decay rather than to go through a minimum. The steep decay up to about 1 sec was followed by a smaller slope of approximately -1. Appearance and disappearance of the needle crystals was so fast that it was not possible to

follow accurately by eye, but the disappearance was about at 1 sec. The region of -1 slope is attributed to high-field growth of oxide as for titanium (32).

Current density transients for potential step experiments in 1N $HClO_4$ are presented in Fig. 6. Again, the initial current density is ohmically limited and the knee of the curve corresponds to Sand's equation, although, in this case, the calculated supersaturation ratio is unity for a $Fe(ClO_4)_2$ solubility of 3.85×10^{-3} mole/cm^3 (31). Salt crystals were not visible in the experiments in 1N $HClO_4$.

Sulfate Electrolytes.--The Potentiodynamic Behavior of iron in sulfuric acid is similar to that in perchloric acid (Fig. 4). The passivation potential is also close to the same value for positive and negative sweep directions.

An interesting experiment, which will be described here, on the effect of convection in 6N H_2SO_4 was, however, carried out. On the positive sweep, electrolyte was jetted into the cavity with an eyedropper, with the result that the potential for passivation was extended above the normal passivation potential. Results are shown in Fig. 7. As soon as the electrolyte jet was stopped, passivation occurred. The slight decrease in current density below the ohmic limit starting at 0.4 V is because salt passivation occured at the corners of the anode. The subsequent plateau is due to a convective mass transport limit. On the negative sweep, after the cavity had been flushed with bulk solution, the current density peaked at the ohmic limit as the potential passed through the passivation potential.

Current density decay curves for iron potentiostated in 6N sulfuric acid

have already been presented (22). The behavior is generally similar to that in perchloric acid and will not be further discussed here.

Potentiostatic step-potential current density transients for 1N Na_2SO_4 are given in Fig. 8. Behavior is similar to that in acid solutions; below the passivation potential, only salt passivation occured, but above, oxide passivation occurred as well. The amount of supersaturation was smaller in comparison to acid solutions. The final limiting-current-density decay also fell below equation 6. The apparent lower ferrous salt solubility for both modes of mass transport may be due to formation of a basic sulfate.

Although study of the passivation potential was not an objective in this work, values observed were generally in agreement with the relation (33)

$$\phi_p = 0.40 - 0.085\ pH \qquad (8)$$

Kinetics and Mechanisms of Crystallization and Passivation.--Salt film precipitation had numbers of complexities that were observed during the course of the investigation. The most striking was that often visible crystals would start at the periphery of the anode, propagate part way toward the center, and stop abruptly. The area covered with visible crystals decreased with increasing potential as shown in Fig. 9 for HCl and H_2SO_4 solutions. At the point in time at which the visible crystals stopped in H_2SO_4 solutions, there was a sudden drop in current density. This is illustrated in Ref. (22), Fig. 1, at a time of about 0.3 sec for the potential of 0.5 V. The proposed explanation is that supersaturation rises to the point that microcrystals nucleate instantaneously over the remaining uncovered surface.

In the case of the higher concentrations of $HClO_4$, even more complex

behavior was noted. Ghost-like crystals were seen to nucleate all over the surface at a time τ^*, to be followed by larger needle crystals growing in from the periphery. Before these larger crystals reached the center, they dissolved on their outer rim so that a diminishing-size ring of visible crystals moved into the center and disappeared. The two sets of crystals may be different hydrates, but salt crystallization kinetics was not the primary objective of this investigation and was not pursued in depth experimentally. Calculations of salt film thickness (based on Ref. (22), Table III and experimental i and τ^*) show that the higher the potential, the thinner the film, and the lower the acid concentration, the thinner the film. The latter explains why crystals were not observed in 1N $HClO_4$; the salt film thickness was less than the wave length of light. For 5N $HClO_4$ and a potential of 0.24 V, a salt film thickness of 13 μm was calculated, and for 0.44 V, a thickness of 6 μm from Ref. (22).

Current density oscillations were observed near the passivation potential in H_2SO_4 and $HClO_4$ as have been reported by others (3). In the more concentrated solutions a very striking oscillatory growth of salt crystals was observed. The salt crystals grew after the current rise and disappeared when the current decayed.

It is now appropriate to consider how oxide passivation is achieved. The thesis is presented here that for iron in these concentrated $HClO_4$ and H_2SO_4 solutions, it is not possible to achieve oxide passivity without first forming the prepassivation salt film. For oxide formation to occur, the surface potential must equal or exceed the passivation potential,

$$\phi_e + \eta_a \geq \phi_p \qquad (9)$$

For $\phi^{\circ}_{e} = -0.44$ V and $\phi_{p} = 0.40$ V at pH = 0 (equation 8), the activation overpotential must therefore exceed 0.84 V for oxide passivation. Tafel kinetics

$$i = i_{o} \exp(\beta \eta_{a}) \tag{10}$$

and values of $i_{o} \approx 10^{-6}$ A/cm^2 and $\beta = 38.9$ V^{-1} (29) give an extrapolated corrosion current density of ~10^{8} A/cm^2 for this overpotential. While this value is perhaps beyond the region of applicability for Tafel kinetics, it is clear that sufficient surface overpotential could not be achieved because of electrolyte ohmic resistance.

Precipitation of a salt film, however, can cause two major changes which could allow oxide passivation: decrease of the current density by limiting Fe^{++} transport, and increase of the local pH at the metal surface due to electrolytic migration of H^{+} away from the surface. Ample evidence of decrease in current density by salt precipitation has been given in this paper. Hydrogen ion may be transported out of the pores in the salt layer by a mechanism described by Wagner (34).

Transport of three ionic species must be considered in the electrolyte in the pores of the salt layer, H^{+}, Fe^{++}, and ClO_{4}^{-}. Neglecting oxide formation at the metal surface, effects of hydrolysis of the ferrous salt, and assuming for the moment a quasi-steady-state, one-dimensional, transport condition, the flux of H^{+} would be zero

$$j_{H} = -D_{H} \frac{dC_{H}}{dx} - \frac{F}{RT} D_{H} C_{H} \frac{d\phi}{dx} = 0 \tag{11}$$

The flux of Fe^{++} is not zero because it is formed at the metal surface by corrosion, and it precipitates and dissolves in the salt layer. The flux of

ClO_4^- is not zero because it precipitates and dissolves in the salt layer. Integration of equation 11 gives

$$\ell n\left(C_{H2}/C_{H1}\right) = -\frac{F}{RT}\left(\phi_2 - \phi_1\right) \tag{12}$$

From the definition of pH, and a temperature of 25°C.

$$\Delta pH = \frac{\Delta\phi_s}{0.059} \tag{13}$$

Combination of equations 13 and 8 gives

$$\phi_p = 0.40 - 1.44\ \Delta\phi_s \tag{14}$$

Equation 13 gives the change in pH across the salt film as a result of a potential drop in the pores according to the above conditions, and equation 14 gives the local passivation potential at the metal surface as modified by this pH change.

Consider data from Fig. 4 to make an example calculation. The applied potential at a current density of ~0.5 A/cm^2, just at the instant before passivation, is about 0.6 V. The potential on the ohmic limited line at a current density of 0.5 A/cm^2 is about 0.1 V. This potential is the sum of the reversible potential, activation overpotential, and electrolyte ohmic drop. The difference of 0.5 V assumed across the salt film gives a pH change of 8.5, according to equation 13, and a passivation potential of -0.32 V, according to equation 14. This passivation potential is about 0.3 V more negative than the required electrolyte iR-free potential in Fig. 4. Thus, for the starting assumptions, there is sufficient decrease in the passivation potential to obtain passivation under the salt layer. Oxide formation at the surface and hydrolysis of the ferrous salt in solution in the diffusion layer would, however, act to decrease the available margin.

The potential drop in the solution in the salt layer can be approximated by

$$\Delta\phi_s = \frac{it}{\kappa_s \theta} \tag{15}$$

For $\Delta\phi_s$ = 0.5 V, i = 0.5 A/cm^2 and t ≈ 10 μm from above, and κ_s ≈ 0.1 Ω^{-1} cm^{-1} for saturated $Fe(ClO_4)_2$ solution, θ is 0.01. Jaenicke, et al., (35), similarly report a 1% porosity for AgCl films.

The oscillatory phenomena near the passivation potential can be explained by the pH changes at the metal surface accompanying the salt film. After salt precipitation, increase in local pH, and oxide passivation, the current density decreases to a low level. The salt is no longer generated at the metal surface, and it then dissolves. Acid penetrates to the metal surface increasing the passivation potential, and the oxide dissolves. The cycle then repeats. The characteristic time for the pH change in the pores is on the order of

$$\tau = \frac{t^2}{D}$$

which for t ≈ 10 μm and D ≈ 10^{-5} cm^2/sec is about 10^{-1} sec. This time is short compared to the 15 sec in Fig. 4 from salt passivation to oxide passivation. Therefore, use of the steady-state flux equation 11 is justified for a first order approximation.

A definitive reason has not yet been obtained for the lack of passivation with convection shown in Fig. 7, although several possibilities are suggested. First, the potential drop across the salt film is seen to be about 0.35 V at the point that the solution jet was stopped. The shift in passivation potential is therefore (-1.44)(0.35) = -0.5 V. The difference between the passivation potential and the iR-free metal surface potnetial is much larger

(0.7 V) so that passivation cannot be achieved. Second, the salt layer next to the metal may become anhydrous at the higher electric field from the convection-caused higher current density. Third, in order for oxide passivation to occur, the ratio of the current densities for corrosion and oxide formation should be less than a number near unity so that oxide nuclei are not undermined as fast as they are formed. It is clear that many detailed questions remain to be answered by further experimentation and by more rigorous modeling. This investigation is continuing.

Conclusions

Ferrous salt films form on iron in 1 normal or greater concentration perchlorate and sulfate solutions for anodic potentials and current densities greater than threshold values determined by mass transport conditions.

Below the passivation potential a salt film remains, and a limiting current density for iron dissolution is determined by mass transport conditions.

Above the passivation potential an oxide film subsequently forms underneath the salt film and causes passivation, then unaffected by convection.

Analysis of kinetic and transport conditions under and within the salt films shows that the salt films are necessary precursors to oxide passivation in perchloric and sulfuric acid solutions.

Oscillatory phenomena observed during passivation of iron can be explained by formation and dissolution of salt films coupled to changes in pH under the salt films due to mass transport.

Acknowledgment

This investigation was supported by the Office of Naval Research (N00014-76-C-0495). The experimental work was carried out by S. G. Chan.

Nomenclature

a = a constant

C = concentration, mole/cm^3

d = depth, cm

D = diffusion coefficient, cm^2/sec

F = the Faraday, 96,500 C/mole

i = current density, A/cm^2

j = flux, mole/cm^2 sec

ℓ = length, cm

r = radius, cm

R = gas constant

t = thickness, cm

T = temperature, deg K

w = width, cm

x = distance, cm

z = equiv/mole

Greek:

β = exponential constant in Tafel equation, V^{-1}

κ = conductivity, ohm^{-1}cm^{-1}

θ = fraction voids

τ = time, sec

ϕ = potential, volts

Subscripts:

a = activation

e = electrolyte or equilibrium

H = hydrogen ion

i = inside

L = limiting

o = outside, exchange current density on i

p = passivation

s = saturation, salt film

1 = metal surface

2 = bulk solution at outer boundary of diffusion layer

References

1. W. J. Muller, Trans. Faraday Soc., 27, 737 (1931).
2. W. J. Muller, Die Bedeckungstheorie der Passivitat der Metalle, Verlag Chemie, Berlin, 1933.
3. J. H. Bartlett, Trans. Electrochem. Soc., 87, 521 (1945).
4. J. H. Bartlett and L. Stephenson, J. Electrochem. Soc., 99, 504 (1952).
5. M. Serra and S. Feliu, Proc. 6th Meeting, CITCE, 360-370 (1955).
6. Sand, Phil. Mag. VI, 1, 45 (1901).
7. M. Froment, M. Keddam, and P. Morel, Compt. Rend., 253, 2529 (1961).
8. K. Schwabe, Z. Phys. Chem., 215, 343 (1960).
9. R. C. Williamson and J. G. Hines, Corros. Sci.,
10. J. G. Hines, Electrochimica Acta, 10, 225 (1965).
11. J. Tousek and M. Prazak, Coll. Czech. Chem. Commun., 31, 1429 (1966).
12. A. Pigeaud and H. B. Kirkpatrick, Corrosion, 25, 209 (1969).
13. Yu. P. Abakumova and N. N. Milyutin, Zhurnal Prikladnoi Khimii, 45, 796 (1972) (translation).
14. W. Lorenz, Z. Physik. Chem., 20, 95 (1959).
15. T. R. Beck, Paper 99 presented at The Electrochemical Society Meeting, Boston, Mass., Oct. 7-11, 1973.
16. H. C. Kuo and D. Landolt, Electrochimica Acta, 20, 393 (1975).
17. H. C. Kuo and D. Landolt, Corros. Sci.,
18. T. P. Hoar, "Modern Aspects of ELectrochemistry," No. 2, J. O'M. Bockris, Editor, p 262, Butterworths, London (1959).
19. D. A. Vermilyea, "Advances in Electrochemistry and Electrochemical Engineering," Vol. 3, P. Delahay and C. W. Tobias, Editors, John Wiley, New York (1963).
20. Ya. M. Kolotyrkin, Mendeleev. Chem. J., 20, pp. 59-70, (Eng. trans.), (1975).
21. I. L. Rosenfeld, I. S. Danilov, and R. N. Oranskaya, J. Electrochem. Soc., 125, 1729 (1978).

22. R. Alkire, D. Ernsberger, and T. R. Beck, J. Electrochem. Soc., 125, 1382 (1978).

23. J. S. Newman, J. Electrochem. Soc., 113, 501, (1966).

24. G. Kortum, "Treatise on Electrochemistry," 2nd Ed., p 456, Elsevier, New York (1965).

25. K. E. Heusler, Z. Elektrochem., 62, 529 (1958).

26. J. O'M. Bockris, D. Drazic, and A. R. Despic, Electrochem. Acta, 4, 325 (1961).

27. E. J. Kelly, J. Electrochem. Soc., 112, 124 (1965).

28. R. J. Chin and K. Nobe, J. Electrochem. Soc., 119, 1457 (1972).

29. E. McCaffery and N. Hackerman, J. Electrochem. Soc., 119, 999 (1972).

30. R. S. Cooper and J. H. Bartlett, J. Electrochem. Soc., 105, 109 (1958).

31. W. F. Linke (revision of Seidell), "Solubilities," Vol. I, 4th Ed., Am. Chem. Soc., Wash., DC (1958).

32. T. R. Beck, Corrosion 30, 408 (1974).

33. M. Pourbaix, "Atlas of Electrochemical Equilibria," p 315, Pergamon Press, New York (1966).

34. C. Wagner, J. Electrochem. Soc., 101, 181 (1954).

35. W. Jaenicke, R. P. Tischer, and H. Gerischer, Z. Elektrochem., 59, 448 (1956).

List of Figures

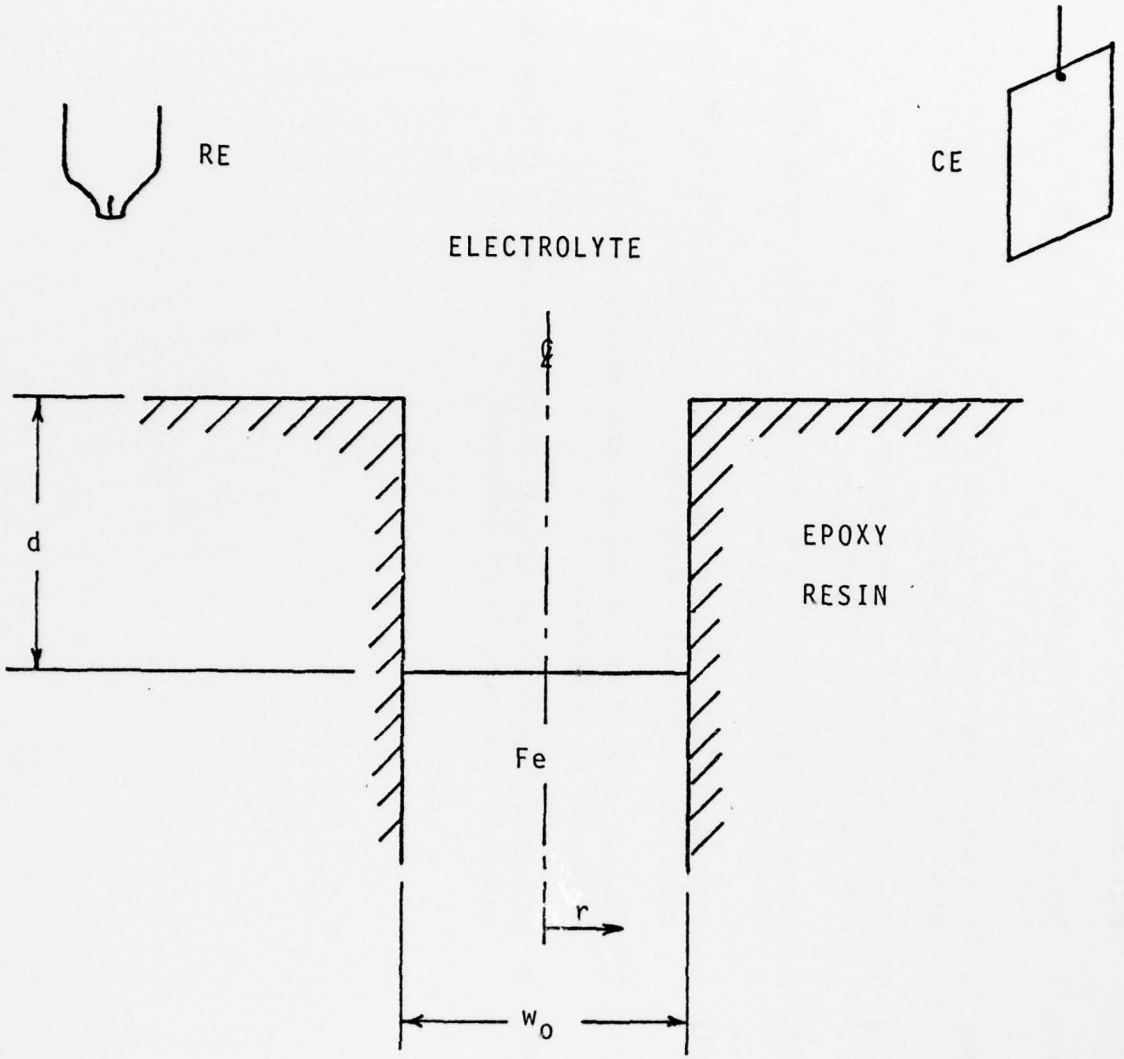

Fig 1

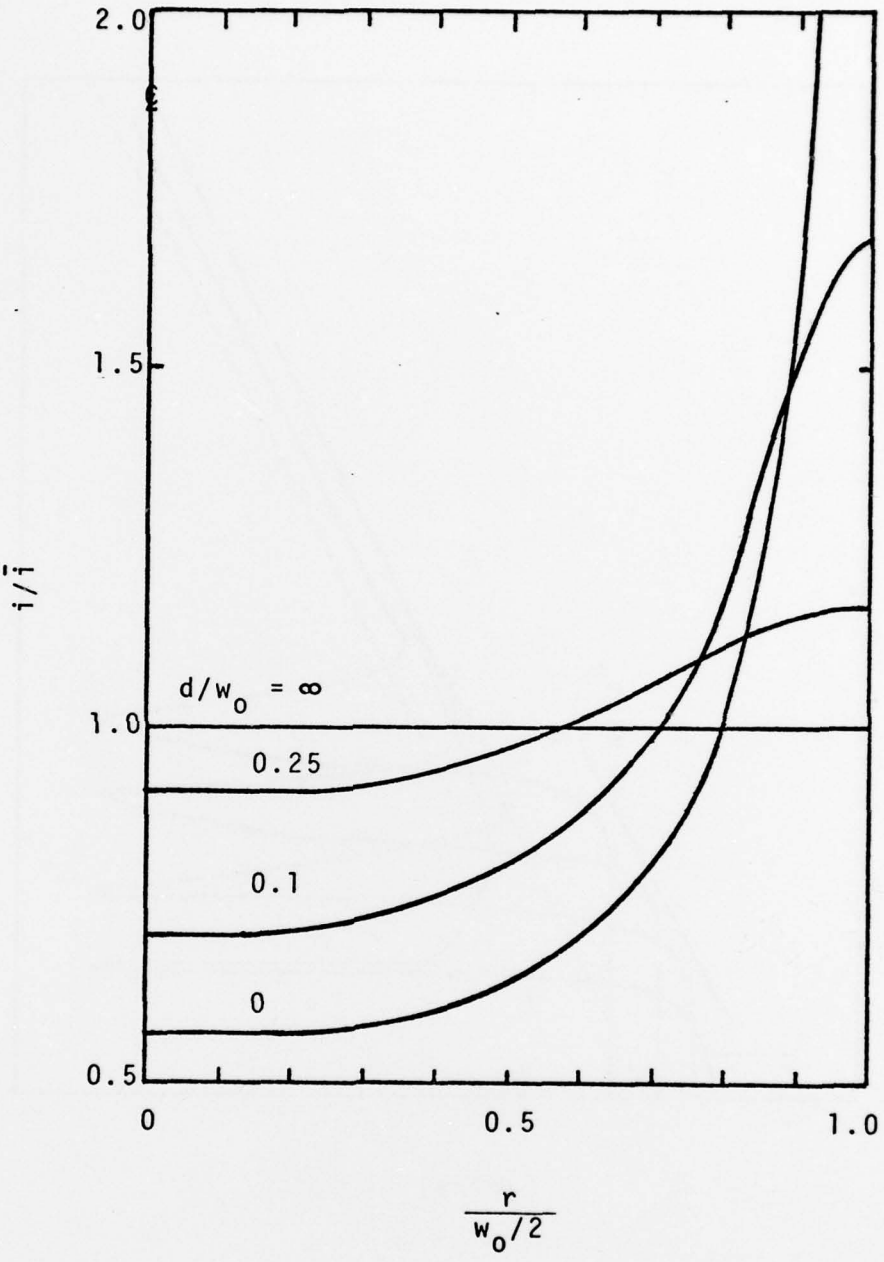

Fig 2

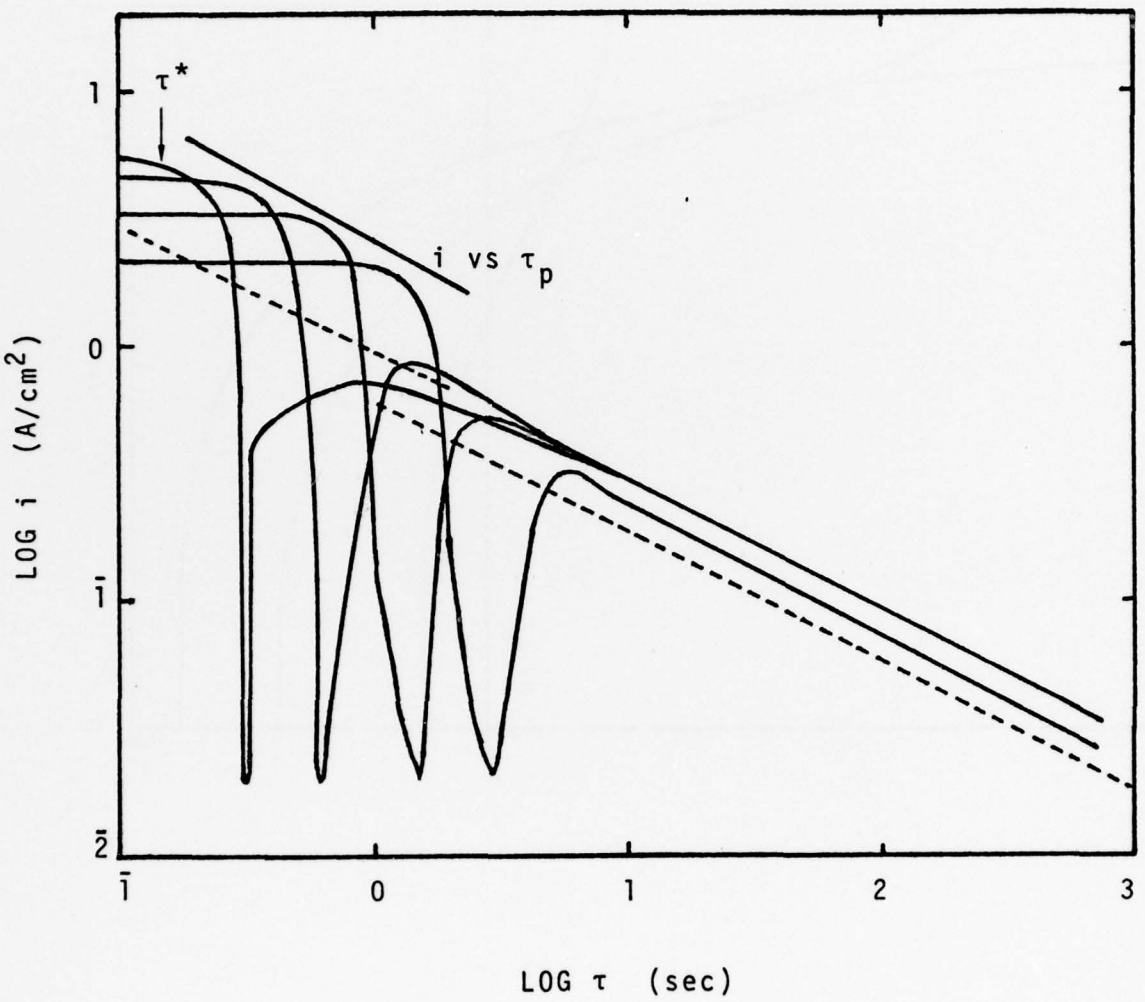

Fig 3

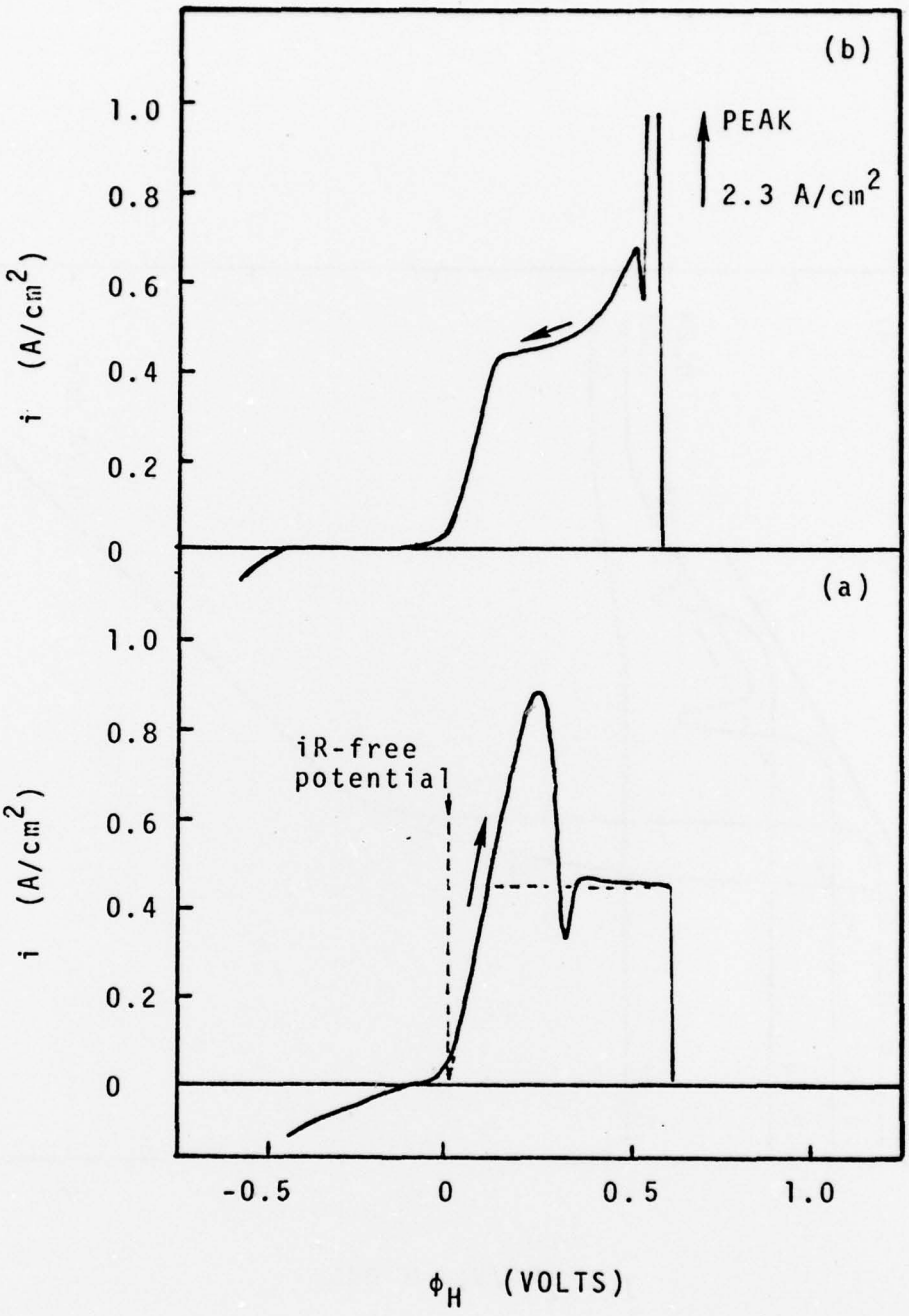
(b)
PEAK
2.3 A/cm²
1.0
0.8
0.6
0.4
0.2
0
i (A/cm²)
(a)
iR-free
potential
-0.5
0
0.5
1.0
φH (VOLTS)

Fig 4

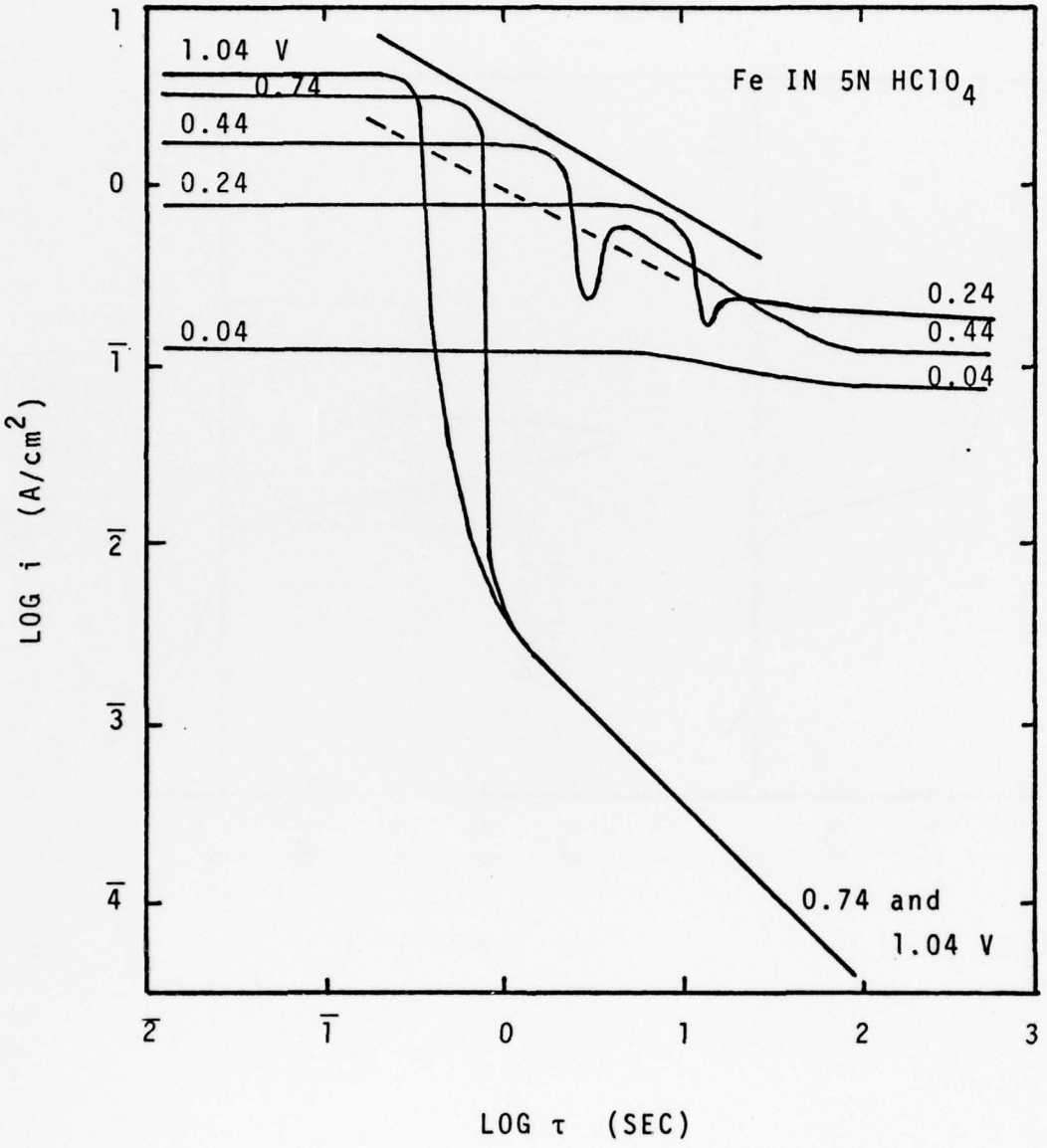
1.04 V
0.74
0.44
0.24
0.04
Fe IN 5N HClO4
0.24
0.44
0.04
0.74 and
1.04 V
1
0
$\bar{1}$
$\bar{2}$
$\bar{3}$
$\bar{4}$
$\bar{2}$
$\bar{1}$
0
1
2
3
LOG i (A/cm^2)
LOG τ (SEC)

Fig. 5

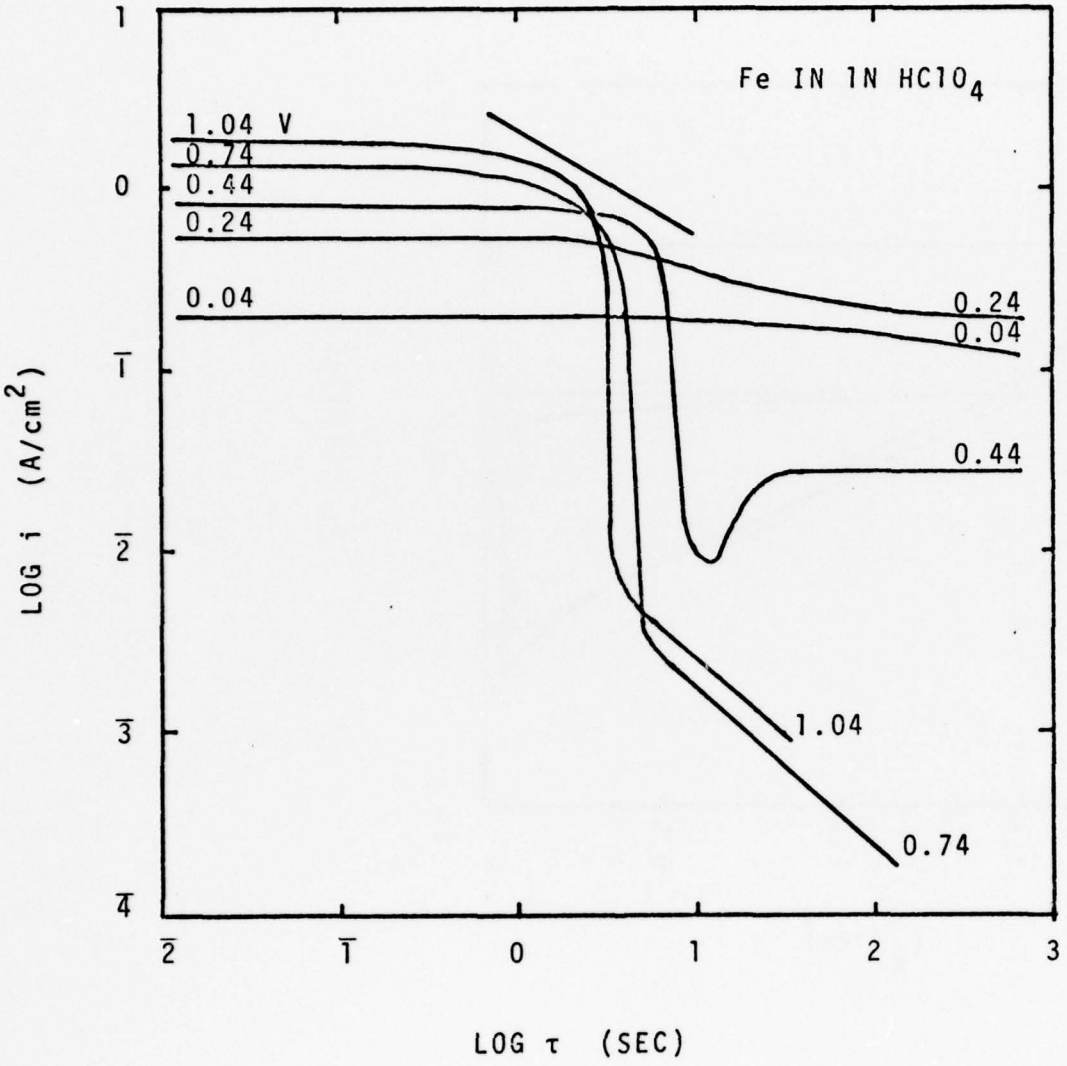
Fe IN 1N HClO4
1.04 V
0.74
0.44
0.24
0.04
0.24
0.04
0.44
1.04
0.74
1
0
$\bar{1}$
$\bar{2}$
$\bar{3}$
$\bar{4}$
$\bar{2}$
$\bar{1}$
0
1
2
3
LOG i (A/cm^2)
LOG τ (SEC)

Fig 6

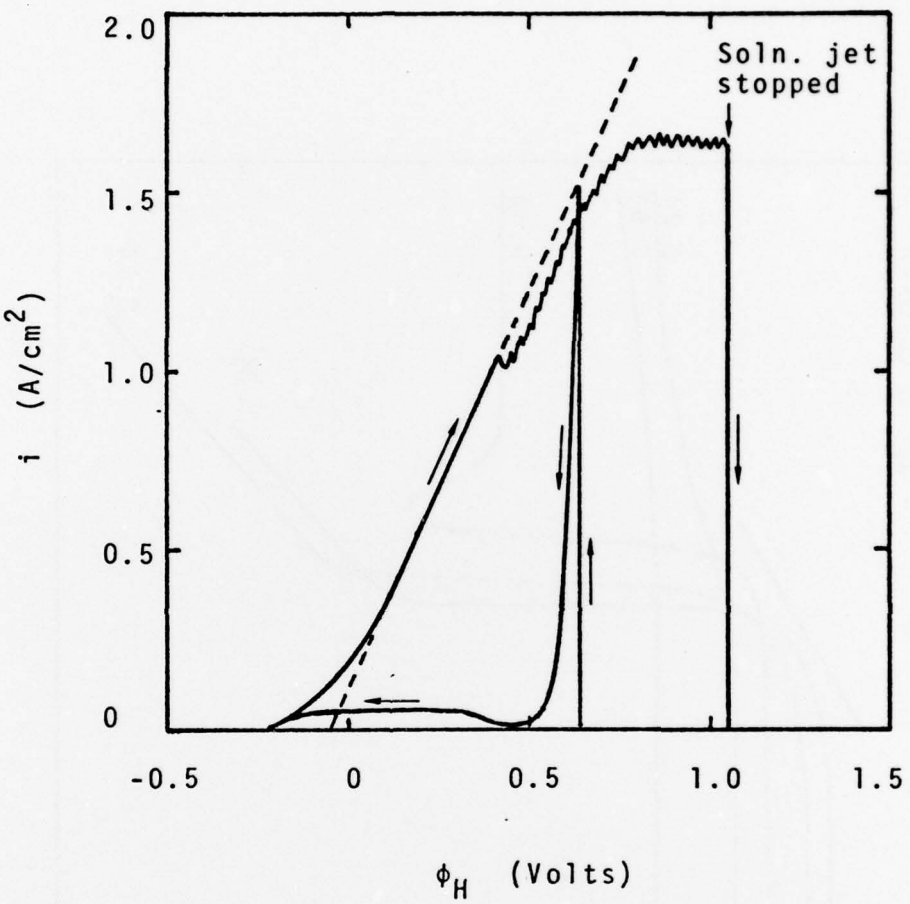

Fig. 7

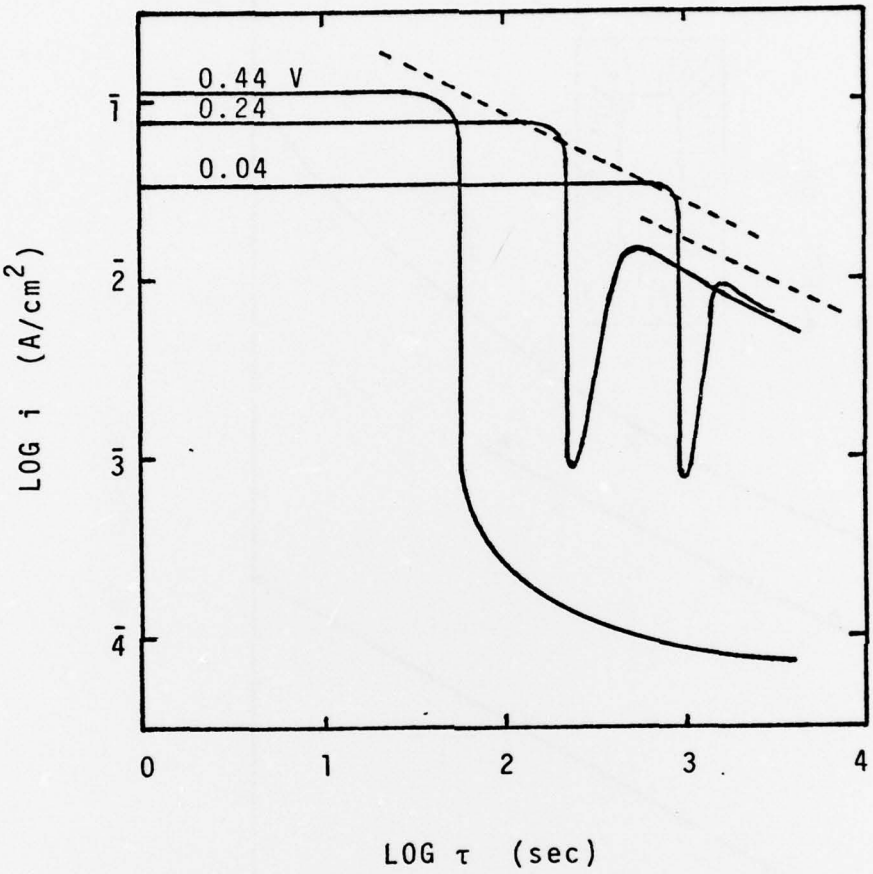

Fig. 8

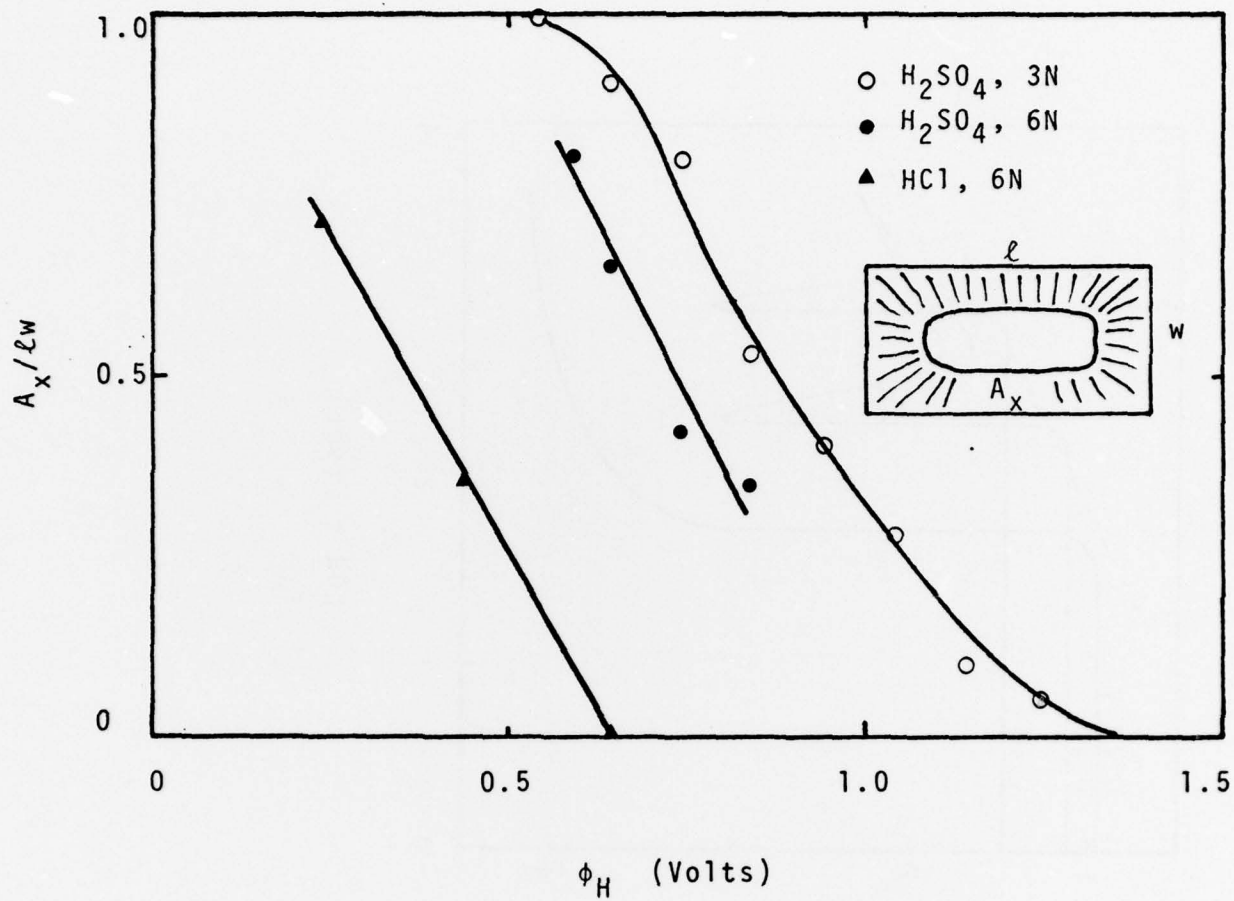
1.0
0.5
0
0
0.5
1.0
1.5
$A_x/\ell w$
ϕ_H (Volts)
○ H_2SO_4, 3N
● H_2SO_4, 6N
▲ HCl, 6N
ℓ
w
A_x

Fig. 9